Journal of Physics Communications

PAPER

Design of open devices based on multi-folded transformation optics

Chengfu Yang[1,2], **Ming Huang**[1,3], **Jingjing Yang**[1,2,3], **Fuchun Mao**[1,2] and **Peng Li**[1,2]

[1] School of Information Science and Engineering, Yunnan University, Kunming 650091, People's Republic of China
[2] Wireless Innovation Lab. of Yunnan University, Kunming 650091, People's Republic of China
[3] Authors to whom any correspondence should be addressed.

E-mail: huangming@ynu.edu.cn **and** yangjingjing@ynu.edu.cn

Keywords: multi-folded transformation optics, complementary medium, remote control, finite element method

OPEN ACCESS

RECEIVED
17 February 2020

REVISED
25 February 2020

ACCEPTED FOR PUBLICATION
23 March 2020

PUBLISHED
14 April 2020

Abstract

Open devices with homogeneous material parameters are proposed and designed based on multi-folded transformation optics, including open cloak device, open field concentrator and open field amplifying device. In comparison with the previous transformation devices, the proposed open devices possess open windows with compact and embedded structures, providing a flexible approach for remote control or upgrade. The open cloaking devices can hide arbitrarily shaped/sized object in the core region, making it disappeared in visually for the outside viewers, while the open field concentrator can enhance or store EM energy in the core region, and the open field amplifying device can magnify the scattering field of a small object, generating an bigger illusory image with differential material parameter and size. The effectiveness and correctness of the proposed devices are validated by the numerical results obtained based on the commercial finite element software COMSOL Multiphysics. Such scheme is believed to find potential applications in remote controlling with impressive new functions.

1. Introduction

AS an ingenious mathematical approach, transformation optics (TO) [1–6] provides a powerful and convenient way to control the electromagnetic (EM) fields arbitrarily, arousing much attentions in the past two decades. Based on this methodology, novel devices with varied functions and applications have been proposed, designed and experimented with an unprecedented prosperity, including invisible cloaks [7–13], concentrators [14–18], illusory devices [19–28] and antennas [29–35] etc. The most striking device among them is invisible cloak, where some properly designed materials are utilized to direct the EM waves propagates smoothly around an arbitrarily shaped object, making the entire device (including the coated object) become invisible for the outside viewers. However, since the EM waves are guided by the coated materials, no wave penetrate into the hidden region, making it impossible for the coated object to interact with the outside world. Furthermore, the coated object cannot move freely in such an enclosed device, making it difficult to meet the needs of replacement or upgrade. In order to overcome these drawbacks, an external cloak that hide an object at a certain distance was proposed by Lai *et al* [12], where complementary medium and 'anit-object' was used to cancel the scattering field generated by the pre-defined hidden object. Additionally, by adding another specific anti-object into the complementary medium, the external cloak acts as an illusion device [19] that makes one object looks like another. However, such an extraordinary device lacks of flexibility and it is merely invisible for an object with specific shape, size and location, i.e., any variation of these factors may greatly deteriorate the stealth effect of the device. It is worth seeking a way to hide an object with arbitrarily shapes or sizes as well as material exchange with the outside world.

As another attractive TO based device, field concentrator can increase and store the EM energies in the core region of the device, and it may find potential applications in solar cells or EM sensors. Since the external EM fields around the concentrator is undisturbed, the entire device acts as an ideal invisibility cloak for an outside viewer. Meanwhile, the concentrator also acts as an illusion device that can render a small object located at the core material to look like another bigger object [14, 16]. Due to this magnifying effect, even minimal divergence or gaps in the core region will result in a deterioration of the desired performance. Furthermore, it is hard to check or predict the

fabricating quality of the core materials when it was fully coated by a properly designed material, let alone replacing or upgrading the internal core material. Therefore, it makes sense to design a concentrator or amplifying device with an open structure, meeting remotely controllable, reciprocal and upgradeable demands of the modern society.

In this paper, based on the multi-folded transformation optics, novel open devices with homogeneous parameters are proposed and designed. The open property allows the hidden object coated by the proposed devices to interact with the outside world and provides a way of remote control or upgade. This open property is generated by compactly embedded segments instead of isolated components, differentiating our study from previous work and providing a robust application in a motion circumstance. Three examples are provided to validate the effectiveness of the proposed open devices. First, an open cloak device is introduced to hide an arbitrarily shaped object which can keep stable or move freely in the hidden region. The results show that the invisibility of the proposed open cloak keeps well, and it can hide objects with arbitrary shapes or positions. A more significant feature is that the structure of the open cloak is compact and integral, which means that it is more stable and robust, and more suitable to be used in a motion circumstance. Second, an open field concentrator that has most area of the core region opened to the outside world is presented. The EM waves are increased perfectly in the core region, indicating that the concentrator has a field enhancement effect. The simulation results show that this enhancement effect is independent of the incident wave direction or the stimulus source. Finally, by embedding a dielectric object into the core region of the proposed open filed concentrator, an open amplifying device is proposed and designed, from which a small dielectric object located at the core region is amplified to a larger image object visually with a different material property in the background medium (air). Full-wave finite element simulations validate the expected behaviors of our proposed devices. It is believed that the proposed opening devices have prospectively potential applications in antennas and propagation fields, including antenna/radar stealth, target camouflage or illusion, novel electromagnetic field sensor or device designing and fabrication etc. Furthermore, it provides a flexible way for remotely controlling the electromagnetic wave.

2. Open device design

According to TO theory, the permittivity and permeability tensors in the virtual space and the physical space are governed by:

$$\varepsilon' = \Lambda\varepsilon\Lambda^T/\det\Lambda,\ \ \mu' = \Lambda\mu\Lambda^T/\det\Lambda. \tag{1}$$

where Λ is the Jacobian transformation matrix between the local distorted coordinates in the virtual space and the Cartesian coordinates in the physical space, $\det\Lambda$ is the determinant of Λ.

Figure 1 demonstrates the schematic diagram of our proposed open devices. All of these devices are obtained by two transformation steps. Firstly, a stretching or compressing transformation method is utilized to transform a virtual space into a conventional device with an enclosed structure, including invisible cloak, concentrator, and amplifying device etc. Subsequently, by employing the multi-folded transformation optics, these conventional devices are further folded and compressed into open devices with a compact and integral structure while maintaining identical performance.

To start with the open cloak device illustrated in figure 1(a), a tiny square PEC (should be small enough for invisibility) is located at the center of the virtual space. The virtual space is divided into eight triangular regions labeled as 1, 2, 3,⋯,8, as the top column shown in figure 1(a). In the step 1, these triangular regions are transformed into eight different regions labeled as 1′, 2′, 3′,⋯,8′ respectively, and the original tiny square PEC is mapped into a bigger one, as the middle column shown in figure 1(a). Therefore, a conventional homogeneous cloak is obtained from the step 1.

In the step 2, we choose two polygons $B_2E_2A_1G_0B_1$ and $B_2F_2C_1H_0B_1$ that are symmetric with respect to the X-axis (middle panel of figure 1(a)) in the conventional cloak and further transform them into polygons $E_2E_1G_0A_1$ and $F_2F_1H_0C_1$ (bottom panel of figure 1(a)). Therefore, an open window is generated in the physical space, as shown in the bottom panel of figure 1(a). All the vertexes are fixing during the coordinate transformation except for B_1 and B_2, i.e., B_1 is mapped into G_1 and H_1, B_2 is mapped into G_2 and H_2. Two sub-steps are taken: firstly, the regions $B_2E_2E_1G_0B_1$ and $B_2F_2F_1H_0B_1$ (orange, middle panel of figure 1(a)) are folded into two regions $E_2E_1G_0G_1G_2$ and $F_2F_1H_0H_1H_2$ (yellow, bottom panel of figure 1(a)). The regions $B_2E_2E_1G_0B_1$ and $B_2F_2F_1H_0B_1$ are further divided into the regions $\Delta B_2E_2E_1$, $\Delta B_2B_1E_1$, $\Delta B_1E_1G_0$, $\Delta B_2F_2F_1$, $\Delta B_2B_1F_1$ and $\Delta B_1F_1G_0$, and the polygonal regions $E_2E_1G_0G_1G_2$ and $F_2F_1H_0H_1H_2$are further divided into the regions $\Delta G_2E_2E_1$, $\Delta G_2G_1E_1$, $\Delta G_1E_1G_0$, $\Delta H_2F_2F_1$, $\Delta H_2H_1F_1$ and $\Delta H_1F_1G_0$. Therefore, the sub-step 1 is described as folding the regions $\Delta B_2E_2E_1$, $\Delta B_2B_1E_1$, $\Delta B_1E_1G_0$, $\Delta B_2F_2F_1$, $\Delta B_2B_1F_1$ and $\Delta B_1F_1G_0$ in the conventional cloak into the regions $\Delta G_2E_2E_1$, $\Delta G_2G_1E_1$, $\Delta G_1E_1G_0$, $\Delta H_2F_2F_1$, $\Delta H_2H_1F_1$ and $\Delta H_1F_1G_0$ respectively in the physical space. Secondly, in order to remove the impedance mismatch generated by this folded transformation, a compressed transformation is used, which compressing the regions $\Delta B_2E_2A_1$, $\Delta B_2B_1A_1$, $\Delta B_1A_1G_0$, $\Delta B_2F_2C_1$, $\Delta B_2B_1C_1$ and $\Delta B_1C_1H_0$ (middle panel of figure 1(a), derive from the polygons $B_2E_2A_1G_0B_1$ and $B_2F_2C_1H_0B_1$) in the conventional cloak into the regions $\Delta G_2E_2A_1$, $\Delta G_2G_1A_1$, $\Delta G_1A_1G_0$, $\Delta H_2F_2C_1$, $\Delta H_2H_1C_1$ and $\Delta H_1C_1H_0$

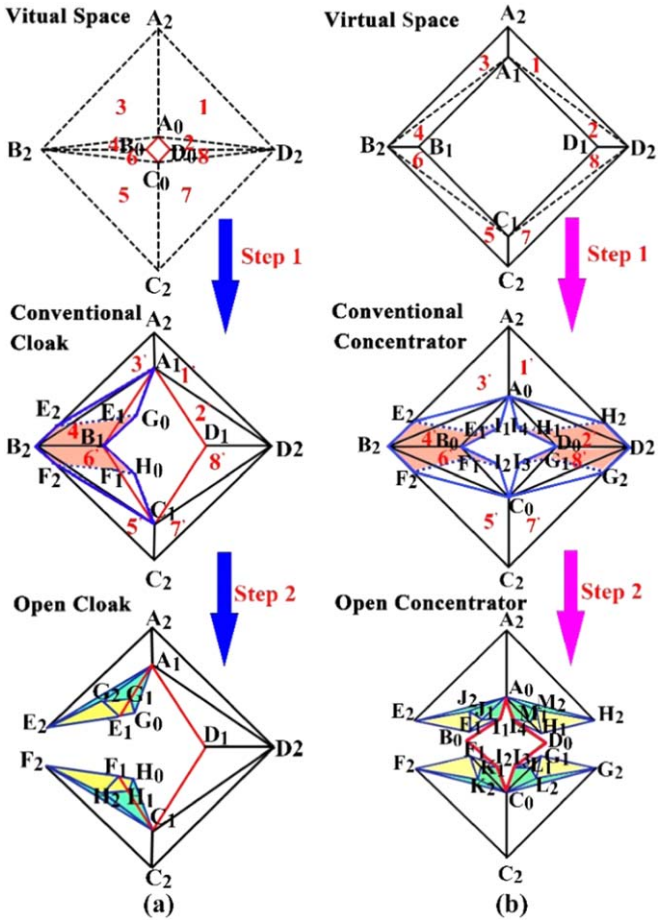

Figure 1. Schematic diagram of the proposed open device. (a)The open cloak, (b) the open concentrator.

(green, bottom panel of figure 1(a)) in the physical space respectively. As a result, the conventional cloak is transformed into an invisible device which has an open window that allows for material and information interaction with the outside world. We named this invisible device as an 'open-cloak' device which can hide an arbitrarily shaped object in the area that is bordered by the inner boundaries of the device.

Similarly, two steps are needed to design an open field concentrator depicted in figure 1(b). In the first step, a square ring in the virtual space is divided into eight triangular regions labeled as 1, 2, 3,⋯,8, as shown in the top panel of figure 1(b). These regions are transformed into regions labeled as1′, 2′, 3′,⋯,8′ respectively, as shown in the middle panel of figure 1(b). Furthermore, the center region bordered by $A_1B_1C_1D_1$ in the top panel of figure 1(b) is compressed into the region $A_0B_0C_0D_0$ in the middle panel of figure 1(b). Afterwards, a conventional concentrator is obtained. In the second step, the polygons $B_2E_2A_0I_1B_0$, $B_2F_2C_0I_2B_0$, $D_2H_2A_0I_4D_0$ and $D_2G_2C_0I_3D_0$ (middle panel of figure 1(b)) in the conventional cloak are transformed into the polygons $E_2E_1I_1A_0$, $F_2F_1I_2C_0$, $H_2H_1I_4A_0$ and $G_2G_1I_3C_0$ (bottom panel of figure 1(b)). Firstly, the orange regions $B_2E_2E_1I_1B_0$, $B_2F_1F_2I_2B_0$, $D_2G_2G_1I_3D_0$, and $D_2H_2H_1I_4D_0$ in the middle panel of figure 1(b) are folded into four yellow color regions $E_2E_1I_1J_1J_2$, $F_2F_1I_2K_1K_2$, $G_2G_1I_3L_1L_2$ and $H_2H_1I_4M_1M_2$ in the bottom panel of figure 1(b), and two open windows are generated in the physical space. Next, compressed transformation is taken to remove the impedance mismatch that coursed by these folded transformations. By further divided the polygons into several triangular regions, transformation mediums with homogeneous material parameters are obtained. Taking the second quadrant component as an example, the regions $\Delta B_2E_2E_1$, $\Delta B_2B_0E_1$ and $\Delta B_0E_1I_1$ derived from the polygon $B_2E_2E_1I_1B_0$ in the conventional cloak are folded into regions $\Delta J_2E_2E_1$, $\Delta J_2J_1E_1$ and $\Delta J_1E_1I_1$ derived from the polygon $E_2E_1I_1J_1J_2$ in the physical space respectively, and regions $\Delta B_2E_2A_0$, $\Delta B_2B_0A_1$ and $\Delta B_0A_0I_1$ derived from the polygon $B_2E_2A_0I_1B_0$ in the conventional concentrator are compressed into the green-colored regions $\Delta J_2E_2A_0$, $\Delta J_2J_0A_0$ and $\Delta J_1A_0I_1$ derived from the polygon $J_2E_2A_0I_1J_1$ in the physical space respectively. Transformations in other quadrants follow a similar approach, which is omitted here for brevity. After the multi-folded transformation, the core region of the concentrator become a star-shaped area, which is bordered by the red lines shown in the bottom panel of figure 1(b).

The schematic diagram of an open field amplifying device is identical to that of an open concentrator and is omitted here for brevity.

In this letter, linear coordinate transformation is employed to achieve transformation mediums with homogeneous material property. Both the virtual space and the transformation space are divided into several triangle regions. The transformation equation between triangles in the physical space and its image in the virtual space is defined as:

$$\begin{bmatrix} x' \\ y' \\ z' \end{bmatrix} = \underbrace{\begin{bmatrix} a & b & 0 \\ c & d & 0 \\ 0 & 0 & 1 \end{bmatrix}}_{\Lambda} \begin{bmatrix} x \\ y \\ z \end{bmatrix} + \begin{bmatrix} e \\ f \\ 0 \end{bmatrix}. \tag{2}$$

where e and f are the non-homogeneous term of linear equation (2), and Λ is the Jacobian matrix governed by the following formula:

$$\Lambda = \begin{bmatrix} a & b & 0 \\ c & d & 0 \\ 0 & 0 & 1 \end{bmatrix} = \begin{bmatrix} x_3' - x_1' & x_2' - x_1' & 0 \\ y_3' - y_1' & y_2' - y_1' & 0 \\ 0 & 0 & 1 \end{bmatrix} \begin{bmatrix} x_3 - x_1 & x_2 - x_1 & 0 \\ y_3 - y_1 & y_2 - y_1 & 0 \\ 0 & 0 & 1 \end{bmatrix}^{-1}. \tag{3}$$

where $(x,\ y)$ and$(x',\ y')$ indicate the before and after transformation coordinates respectively, and 1, 2, 3 represent the vertex order of the triangles. Since the constitutive parameter of the transformation medium is determined by the Jacobian matrix Λ only, it is not required to calculate the non-homogeneous term of linear equation (2).

Thus, the required material parameters of each triangles of the proposed open devices are obtained by substituting corresponding vertex coordinates into equations (3) and (1).

For an open-cloak, the coordinates of the vertexes are $A_2(0,\ 0.04)$, $B_2(-0.04,\ 0)$, $C_2(0,\ -0.04)$, $D_2(0.04,\ 0)$, $A_1(0,\ 0.03)$, $B_1(-0.015,\ 0)$, $C_1(0,\ -0.03)$, $D_1(0.015,\ 0)$, $A_0(0,\ 0.0001)$, $B_0(-0.0001,\ 0)$, $C_0(0,\ -0.0001)$, $D_0(0.0001,\ 0)$, $E_1(-0.0105,\ 0.0089)$, $E_2(-0.0352,\ 0.0048)$, $F_1(-0.0105,\ -0.0089)$, $F_2(-0.0352,\ -0.0048)$, $G_1(-0.0061,\ 0.0178)$, $G_2(-0.0263,\ 0.01026)$, $H_1(-0.0061,\ -0.0178)$, $H_2(-0.0263,\ -0.01026)$, $G_0(-0.0076,\ 0.0093)$, $H_0(-0.0076,\ -0.0093)$. All vertex coordinates are in meters.

As a result, material parameters of the conventional cloak are obtained as:

$$\varepsilon_1' = \mu_1' = \varepsilon_5' = \mu_5' = \begin{bmatrix} 3.99 & -2.99 & 0 \\ -2.99 & 2.4913 & 0 \\ 0 & 0 & 3.99 \end{bmatrix},$$

$$\varepsilon_2' = \mu_2' = \varepsilon_6' = \mu_6' = \begin{bmatrix} 118.7042 & -238.4 & 0 \\ -238.4 & 478.8 & 0 \\ 0 & 0 & 0.0053 \end{bmatrix},$$

$$\varepsilon_3' = \mu_3' = \varepsilon_7' = \mu_7' = \begin{bmatrix} 3.99 & 2.99 & 0 \\ 2.99 & 2.4913 & 0 \\ 0 & 0 & 3.99 \end{bmatrix},$$

$$\varepsilon_4' = \mu_4' = \varepsilon_8' = \mu_8' = \begin{bmatrix} 118.7042 & 238.4 & 0 \\ 238.4 & 478.8 & 0 \\ 0 & 0 & 0.0053 \end{bmatrix},$$

and the material parameters of each triangles bordered by blue lines in the second quadrant are obtained as:

$$\varepsilon'_{E_2G_2E_1} = \mu'_{E_2G_2E_1} = \begin{bmatrix} -14.2245 & -6.0612 & 0 \\ -6.0612 & -2.6531 & 0 \\ 0 & 0 & -1 \end{bmatrix},$$

$$\varepsilon'_{G_1G_2E_1} = \mu'_{G_1G_2E_1} = \begin{bmatrix} -2.2362 & -1.9531 & 0 \\ -1.9531 & -2.1529 & 0 \\ 0 & 0 & -1.5217 \end{bmatrix},$$

$$\varepsilon'_{G_1G_0E_1} = \mu'_{G_1G_0E_1} = \begin{bmatrix} -2.5868 & -1.719 & 0 \\ -1.719 & -1.5289 & 0 \\ 0 & 0 & -1 \end{bmatrix},$$

$$\varepsilon'_{E_2G_2A_1} = \mu'_{E_2G_2A_1} = \begin{bmatrix} 41.2484 & 27.0981 & 0 \\ 27.0981 & 17.8264 & 0 \\ 0 & 0 & 6.0717 \end{bmatrix},$$

$$\varepsilon'_{G_1G_2A_1} = \mu'_{G_1G_2A_1} = \begin{bmatrix} 72.7458 & 146.475 & 0 \\ 146.475 & 294.9437 & 0 \\ 0 & 0 & 0.0199 \end{bmatrix},$$

$$\varepsilon'_{G_0G_1A_1} = \mu'_{G_0G_1A_1} = \begin{bmatrix} 5.8769 & 20.2015 & 0 \\ 20.2015 & 69.612 & 0 \\ 0 & 0 & 2.4627 \end{bmatrix}$$

Due to the structural symmetry of the open cloak, the material parameters of each triangles bordered by the blue lines in the third quadrant are almost identical to that of the triangles in the second quadrant which is symmetric with respect to the X axis, just replacing the off-diagonal elements by $\varepsilon'_{xy(III)} = \mu'_{xy(III)} = -\varepsilon'_{xy(II)} = -\mu'_{xy(II)}$ while keeping the diagonal components unchanged. It should be noted that when calculating the material parameters of the compressed regions $\Delta E_2 G_2 A_1$ and $\Delta G_1 G_2 A_1$ (green-colored region, bottom panel of figure 1(a)), the material parameters of regions 3′ and 4′ must be multiplied, because these compressed regions are obtained from the conventional cloak.

Similarly, for an open concentrator, the coordinates of the vertexes are $A_2(0,\ 0.04)$, $B_2(-0.04,\ 0)$, $C_2(0,\ -0.04)$, $D_2(0.04,\ 0)$, $A_1(0,\ 0.03)$, $B_1(-0.03,\ 0)$, $C_1(0,\ -0.03)$, $D_1(0.03,\ 0)$, $A_0(0,\ 0.01)$, $B_0(-0.\ 01,\ 0)$, $C_0(0,\ -0.01)$, $D_0(0.\ 01,\ 0)$, $E_1(-0.0080,\ 0.002)$, $E_2(-0.036,\ 0.004)$, $F_1(-0.0080,\ -0.002)$, $F_2(-0.036,\ -0.004)$, $G_1(0.0080,\ -0.002)$, $G_2(0.036,\ -0.004)$, $H_1(0.0080,\ 0.002)$, $H_2(0.036,\ 0.004)$, $J_1(-0.0060,\ 0.004)$, $J_2(-0.01333,\ 0.0067)$, $K_1(-0.0060,\ -0.004)$, $K_2(-0.01333,\ -0.0067)$, $L_1(0.0060,\ -0.004)$, $L_2(0.01333,\ -0.0067)$, $M_1(0.0060,\ 0.004)$, $M_2(0.01333,\ 0.0067)$, $I_1(-0.0020,\ 0.007)$, $I_2(-0.0020,\ -0.007)$, $I_3(0.0020,\ -0.007)$, $I_4(0.0020,\ 0.007)$. All vertex coordinates are in meters. The material properties of the conventional concentrator are obtained as:

$$\varepsilon'_1 = \mu'_1 = \varepsilon'_5 = \mu'_5 = \begin{bmatrix} 0.3333 & 0.6667 & 0 \\ 0.6667 & 4.3333 & 0 \\ 0 & 0 & 0.3333 \end{bmatrix},$$

$$\varepsilon'_2 = \mu'_2 = \varepsilon'_4 = \mu'_4 = \varepsilon'_6 = \mu'_6 = \varepsilon'_8 = \mu'_8 = diag(3,\ 0.3333,\ 3),$$

$$\varepsilon'_3 = \mu'_3 = \varepsilon'_7 = \mu'_7 = \begin{bmatrix} 0.3333 & -0.6667 & 0 \\ -0.6667 & 4.3333 & 0 \\ 0 & 0 & 0.3333 \end{bmatrix},$$

and the material parameters of each triangles bordered by blue lines in the second quadrant of the open concentrator are obtained as:

$$\varepsilon'_{E_2J_2E_1} = \mu'_{E_2J_2E_1} = \begin{bmatrix} -39.0247 & -3.3951 & 0 \\ -3.3951 & -0.3210 & 0 \\ 0 & 0 & -1 \end{bmatrix},$$

$$\varepsilon'_{J_1J_2E_1} = \mu'_{J_1J_2E_1} = \begin{bmatrix} -4.8252 & -3.3363 & 0 \\ -3.3363 & -2.5141 & 0 \\ 0 & 0 & -3 \end{bmatrix},$$

$$\varepsilon'_{J_1I_1E_1} = \mu'_{J_1I_1E_1} = \begin{bmatrix} -265 & -242 & 0 \\ -242 & -221 & 0 \\ 0 & 0 & -1 \end{bmatrix},$$

$$\varepsilon'_{E_2J_2A_0} = \mu'_{E_2J_2A_0} = \begin{bmatrix} 912.1111 & 114.7778 & 0 \\ 114.7778 & 114.4444 & 0 \\ 0 & 0 & 1 \end{bmatrix},$$

$$\varepsilon'_{J_1J_2A_0} = \mu'_{J_1J_2A_0} = \begin{bmatrix} 4.1111 & -2.2222 & 0 \\ -2.2222 & 1.4444 & 0 \\ 0 & 0 & 5 \end{bmatrix},$$

$$\varepsilon'_{I_1J_1A_0} = \mu'_{I_1J_1A_0} = \begin{bmatrix} 1.1333 & 2.8 & 0 \\ 2.8 & 7.8 & 0 \\ 0 & 0 & 15 \end{bmatrix}.$$

Due to the structural symmetry of the open concentrator, the material parameter tensors of ach triangles bordered by the blue lines in other quadrants are almost identical to that of the triangles in the second quadrant which is symmetric with respect to the x-axis or the y-axis, just replacing the off-diagonal elements by $\varepsilon'_{xy(I)} = \mu'_{xy(I)} = \varepsilon'_{xy(III)} = \mu'_{xy(III)} = -\varepsilon'_{xy(II)} = -\mu'_{xy(II)} = -\varepsilon'_{xy(IV)} = -\mu'_{xy(IV)}$ while keeping the diagonal elements unchanged.

For the core region of the concentrator, a big square with circum-radius of $a = 0.03$ m is compressed into a small square with radius of $b = 0.01$ m. The transformation equations are defined as:

$$\begin{aligned} x' &= kx, \\ y' &= ky, \\ z' &= z. \end{aligned} \tag{4}$$

where k is the compression ratio of $k = b/a = 3$. Thus, the material parameters of the core region are $\varepsilon' = \mu' = diag(1,\ 1,\ 9)$.

Similarly, when calculating the material parameters of the compressed regions $\Delta J_2 E_2 A_0$ and $\Delta J_2 J_1 A_0$, the material parameters of regions 3′, 4′ must be multiplied respectively, and the material parameters of $\Delta J_1 A_0 I_1$

must multiply the parameters of the core region. The material parameters of the open amplifying device are identical to that of the open concentrator, and it was omitted here for brevity.

3. Numerical simulations and discussion

The commercial finite element software (COMSOL) is adopted to validate the effectiveness and accurateness of the proposed open devices. Simulations are carried out under a transverse electric (TE) plane wave or a cylindrical wave irradiation with a frequency of 10 GHz in this letter.

Let's start with the validation of the proposed open cloak. In figure 2, a unit plane wave normally incident from left to right to investigate the electric field (E_z) distribution around a PEC object or a cloak device. From figures 2(a) and (b), it is observed that the EM waves are smoothly guided by the properly designed materials and the wave fronts are restored well for both the conventional cloak (figure 2(a)) and the proposed open cloak (figure 2(b)). However, when without the cloak device, the scattering field of the PEC object is strong, as shown in figure 2(c). The absence of the scattering field when a PEC object is covered by the coated material validates the invisibility of the proposed open cloak. Two notes should be clarified here: (1) the strong fields in the vicinity of the open window are caused by the surface mode resonance excited by the multiple scattering of EM wave between positive and negative materials; (2) minor distortion of the field around both the conventional cloak or the proposed open cloak is due to the fact that the hidden region is stretched from a small square ring rather than a tiny point. Furthermore, the far field differential RCS (radar cross section) is calculated here to quantitatively examine the invisibility of the proposed open-cloak device, as shown in figure 2(d), where the blue-colored line represents the RCS with a bare square PEC, while the red-colored line and green-colored line indicate the RCS with the conventional cloak and the proposed open-cloak device, respectively. The strong scattering field of a PEC object is almost disappeared when the PEC object is coated by a properly designed cloak device, including the conventional cloak and the open cloak developed here. The greatest reduction occurs at the forward scattering direction.

Next, we investigate the capability of the proposed open cloak to hide different object with different sizes, shapes or locations. Three cases are discussed, and the field distributions of them are calculated when they are without or with the proposed open-cloak device, as shown in figure 3. In the first case, a unit TE plane wave along x-direction is irradiating on an oval-shaped dielectric object with $\varepsilon_o = -1,\ \mu_o = 1$, as shown in figure 3(a). In this case, scattering field is observed, especially in the forward direction. In figure 3(b), the same oval shaped dielectric object is coated by the proposed open-cloak device and subjected to the same TE plane wave. Obviously, the scattering field generated by the object is greatly reduced when the object is covered by the cloak device. Thus, the oval-shaped object become invisible for the outside world. Furthermore, no electric field penetrates into the core region in this case since the inner boundaries colored by the red lines in figure 1(a) is set as PEC. In the second case, a cup-shaped object with $\varepsilon_o = 3.9,\ \mu_o = 1$ is instead of the oval-shaped dielectric object, as shown in figures 3(d) and (e). Similarly, scattering field is observed when the cup-shaped object is directly exposed to the free space (air), as demonstrated in figure 3(d). However, the scattering field is minimized when the object is wrapped by the open-cloak device, and the object become invisible, as illustrated in figure 3(e). All these two cases mentioned above discussed the capability of the open cloak to hide arbitrary dielectric object, regardless of its shape, size or location.

In the third case, we replace the dielectric object with a magnetic medium. Figures 3(g) and (h) demonstrate the field distribution of a star-shaped object of $\varepsilon_o = 1, \mu_o = 20$ when without and with the open cloak respectively. Again, the scattering field caused by the object alone (figure 3(g)) is greatly reduced when it covered with the open cloak device (figure 3(h)). Furthermore, far field differential RCS is calculated for all cases mentioned above, as shown in figures 3(c), (f) and (i), where blue-colored lines indicate the RCS of the bare objects exposed in the air, while the red-colored lines represent RCS with the open-cloaking devices. It is clear that the scattering field is well suppressed when the object is covered by the proposed open device. All discussions above validate the capability of the proposed open cloak device to hide any object regardless of its shape, size or location. In a short word, the invisibility is independent of objects, shapes and positions.

Comparing to a traditional cloak device [1, 3, 7–10], the proposed open cloak provides the capability of material or information convertible with the outer world as well as an external cloak [12]. However, it should be noted that the invisibility of an external cloak is greatly depended on a pre-defined position, shape and size of a hidden object while the proposed device is independent of them, which provides a feasible approach to hide a moving object. Although the concept of open cloak has been proposed by Han *et al* [36–38] in 2010, the inhomogeneity and anisotropy of material parameters was a big challenge for fabrication. In contrast, the homogeneous open cloak proposed here will relax the implementation difficulty of the device. Furthermore, different from the remote device proposed by Zheng *et al* [39], the open cloak device developed here is composed of a compact, embedded and continuously structure which have more robustness to avoid the field perturbation

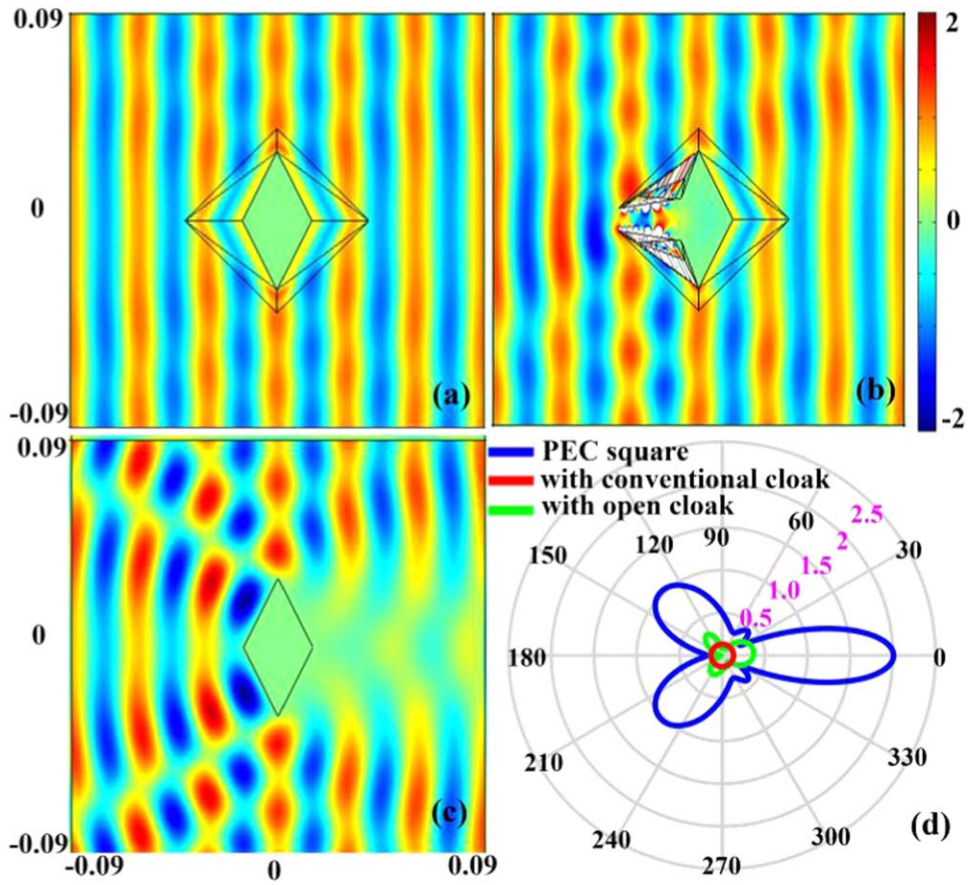

Figure 2. The electric field distributions in 2D TE scattering mode for a PEC circular-shaped object alone and coated by a conventional cloak or an open cloak. (a) Near filed distribution of a PEC object coated by a conventional cloak. (b) Near filed distribution of a PEC object coated by the proposed open cloak. (c) Scattering field of a PEC object in the free space. (d) Comparison of the calculated far field differential RCS (radar cross section) of (a)–(c).

caused by position offset or impedance mismatch that may exists in an isolated structure devices, even in a motion circumstance.

Next, we focus on the validation of the EM field concentration of the proposed open concentrator. Figure 4 illustrates the distribution of the electric field and the total energy density of the developed novel concentrator. In figures 4(a)–(c), a TE plane wave is irradiating on the concentrator along the x-direction, the y-direction and with an oblique incidence angle of $\pi/4$, respectively. It is observed that the EM waves are perfectly focused into the core region of the open concentrator, validating that the field concentrator can be made open (at least partially open) to the outside world while keep the overall performance unchanged. Furthermore, the simulation results indicate that the field concentration is independent of the incidence direction of the electric filed and the device is prominently invisible to the outer world. In figure 4(d), a line source with unit power located at (−0.06 m, −0.06 m) is irradiating on the proposed open concentrator. It is observed that the field concentration effect is also effective under the irradiation of a line source, confirming that this concentration feature is independent of the stimulus source.

Figures 4(e) and (f) demonstrate the total energy density distribution under the irradiation of a TE plane wave and a line source wave respectively. Obviously, the energy density of the EM wave is mainly focused at the center region of the device, which further confirms the prominent concentration-effect of the proposed open concentrator. Three notes differentiate the proposed novel device from the previous remote concentrating device reported by Madni *et al* [18]: (1) the coating region are connected to the top and bottom of the core region in the proposed open-device, while air-gap exists between the core-region and coating region in Madni's work; (2) the components that generate open function are embedded in the coating material, making the proposed open concentrator still have a continuous and compact structure. Thus, it doesn't need to adjust the position of the open window when the device is moved into a new location or it need an upgrade of the core material. For an easy word, it has more robustness; (3) Most of the material parameters are homogeneous and positive, which provides feasibility to implement.

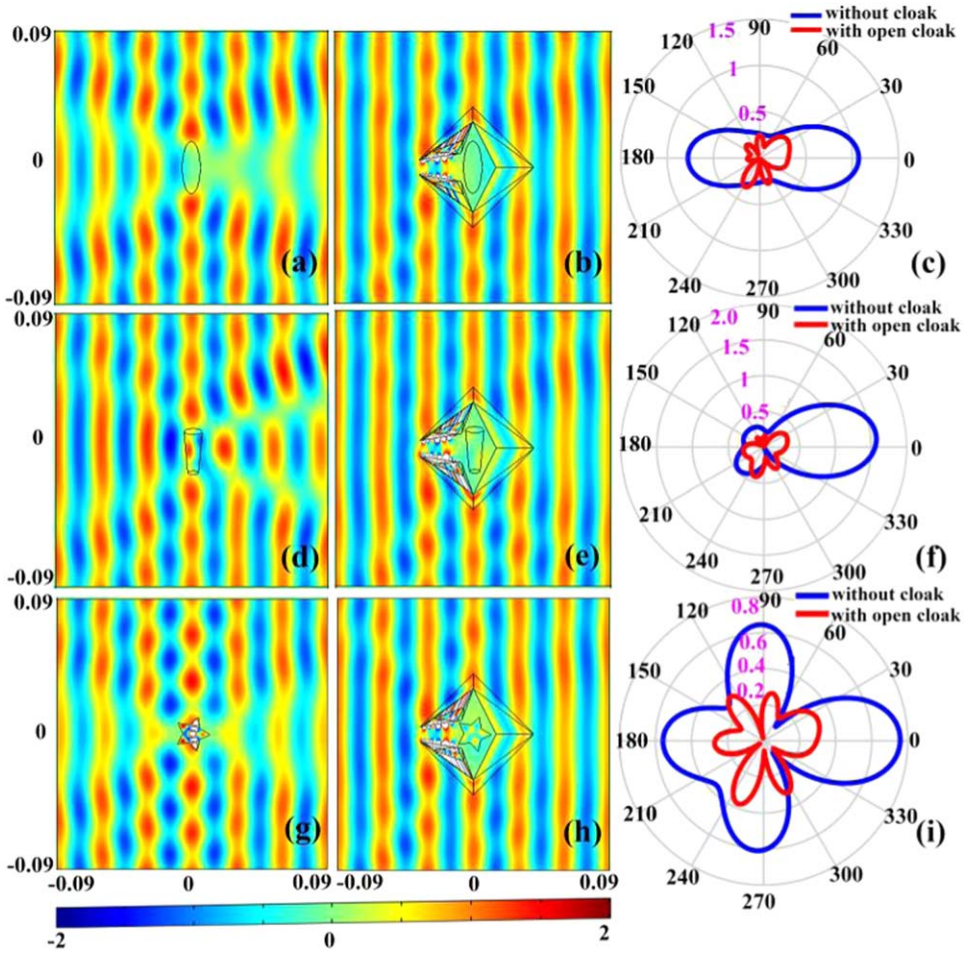

Figure 3. Comparison of the electric field distributions in 2D TE scattering mode for an object alone in the free space and with the open cloak device. (a)An oval-shaped dielectric object with $\varepsilon_o = -1$, $\mu_o = 1$ is directly irradiated by a TE plane wave along the x-direction, demonstrating large scattering, while in (b), the scattering field is greatly reduced when the object is enclosed by the propose open cloak device. (d) A bare cup-shaped dielectric object with $\varepsilon_o = 3.9$, $\mu_o = 1$ is subjected to a unit TE plane wave, while in (e), the same object is covered by the open cloaking device. (g) A star-shaped magnetic object of $\varepsilon_o = 1$, $\mu_o = 20$ is directly exposed to a TE plane wave, while in (h), the same objects are putted inside the open cloaking device. (c) The far field differential RCS of (a) and (b). (f) The far field differential RCS of (d) and (e). (i) The far field differential RCS of (g) and (h).

Next, we further examine the amplifying effect by putting a dielectric object into the core region of the proposed open-concentrating device. We named this device as an 'open-amplifying' device. According to TO method, the material parameters between the virtual space and the transformation space is governed by equation (1). Thus, the relationship of the material parameters between the object embedded in the core region and its virtual image in the free space are defined as $\varepsilon'_{object}/\varepsilon_{image} = \mu'_{object}/\mu_{image} = \varepsilon'_{core} = \mu'_{core} = diag(1,\ 1,\ 9)$.

Figure 5 illustrates the electric field distribution of the object embedded into the core region of the open-amplifying device and its virtual image in the free space. In figure 5(b), a small cup-shaped object with $\varepsilon' = 45,\ \mu' = 1$ is embedded into the core region of the open-amplifying device, while in figure 5(a), a big cup-shaped object with $\varepsilon = 5,\ \mu = 1$ is directly exposed to the irradiation of a TE plane wave. Comparing figure 5(a) with figure 5(b), it is observed that the electric field distribution of them are almost identical, confirming the effectiveness of the proposed amplifying device to amplify an object that is located at the core region of the device. In figures 5(e) and (h), the small cup-shaped object is replaced by a star-shaped object with $\varepsilon' = -1,\ \mu' = 1$ and a circular-shaped object with $\varepsilon' = 27,\ \mu' = 1$ respectively. The virtual images of the star-shaped object and the circular-shaped object in figures 5(e) and (h) are demonstrated in figures 5(d) and (g) with $\varepsilon = -1/9,\ \mu = 1$ and $\varepsilon = 3,\ \mu = 1$ respectively. Again, the identical field distribution of the object in the proposed device (figures 5(e) and (h)) and its virtual image in the free space (5(d) and 5(g)) validates the amplification ability of the proposed open device. To quantitatively examine the performance of the amplifying effect, far field differential RCS of all cases mentioned above are calculated, as shown in figures 5(c), (f) and (i), where the red-colored lines and blue-colored lines indicate RCS of the object embedded in the open-amplifying device and their image in the free space, respectively. Obviously, the blue-colored lines and the red-colored lines

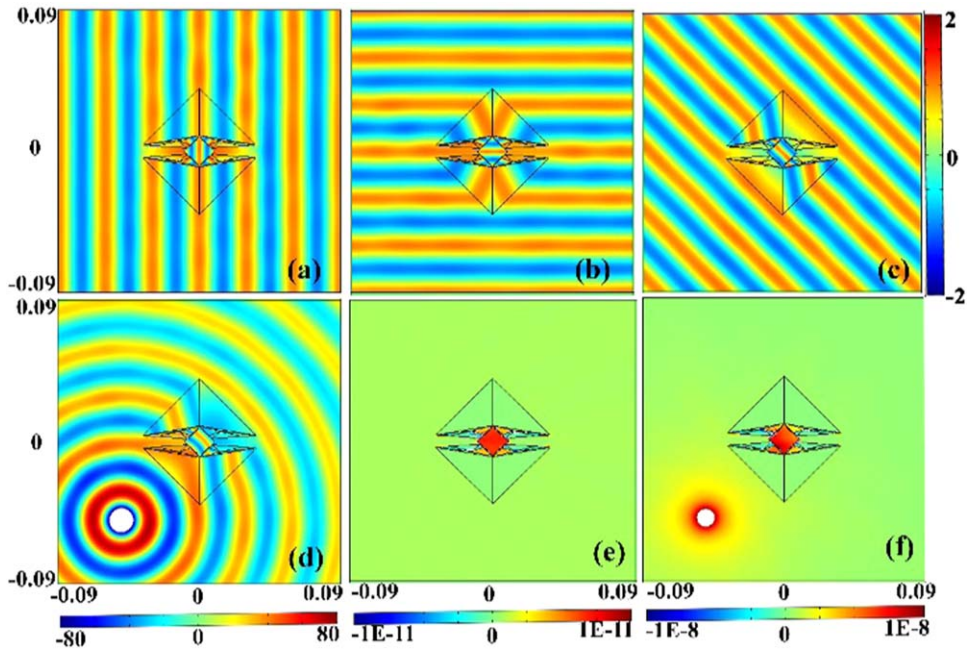

Figure 4. The Electric field distribution (E_z) and the total energy density distribution in the vicinity of the proposed open field concentrator. A TE plane wave is irradiating on the proposed open concentrator along (a) the x-direction, (b) the y-direction, (c) an oblique incidence angle of $\pi/4$. (d) An line source with a unit power located at (−0.06 m, −0.06 m) is illuminating on the proposed open concentrator. Total energy density distribution under the illumination of (e) a TE plane wave, (f) a line source.

almost overlaps and the RCS of them are identical to each other. The simulation results illustrated in figures 5(c), (f) and (i) validate the excellent amplifying effect of the proposed open device.

Finally, a brief discussion on future experiment of such open devices are taken. There is no denying the fact that the highly anisotropic material combined with negative or near-zero values is still a big challenge to fabricate in transient mode. One possible approach is use metamaterial structure with split ring resonators (SRRs) and metal rods [7, 39–41]. Generally, these highly off-diagonal anisotropy values in the x-y plane should be transformed to a diagonal tensor for both permittivity and permeability in the u-v plane (a rotating coordinate system) to facilitate. For example, in a transverse magnetic polarization case, this transformation is given by $\mu^w = \mu_{zz}$, $\varepsilon^{u,v} = [\varepsilon_{xx} + \varepsilon_{yy} \pm \sqrt{(\varepsilon_{xx} - \varepsilon_{yy})^2 + 4\varepsilon_{xy}^2}]/2$, where ε_{xx}, ε_{xy}, ε_{yy} and μ_{zz} are the components of the off-diagonal parameter tensor in x-y plane, ε^u, ε^v and μ^w is the components of the diagonal parameter tensor in the u-v plane. The required mediums can be obtained by carefully tune the geometrical sizes of the metamaterial units and the permittivity of the substrate, which can specifically refer to [39]. However, most of the resonant based implementation have narrow bandwidth and lossy, which sacrifices the performance of the device. Another potential approach is use periodical L–C transmission line network, where relevant capacitors and inductors are used to equivalently realize the required permittivity and permeability mediums [42, 43]. Still, L–C network only valid in the low frequency band (usually below the C-band) where the unit size is far less than working wavelength ($\lambda/20$) and the parasitic effects of lumped components are negligible. Furthermore, the using of graphene to dynamically tune the permittivity by means of chemical doping or gate voltage [44] is a prospective approach to achieve TO-based device, but it is still challenged to tune an anisotropic medium. Fortunately, for a direct current (DC) mode, a remote function cloak was successfully experimented by Chen et. al in [45], where negative resistor network with active elements is used to implement. Therefore, the device proposal here may be find experimental verification soon at DC frequency in future, which may find potential applications in medical and geologic research.

4. Conclusion

In summary, novel open devices with homogeneous properties are proposed and designed, including open invisibility cloak, open field concentrator and open amplifying device etc. The open features of the proposed devices allow for matter and information interaction with the outside, providing a feasible approach for remote control or upgrade of the coated object. Complementary medium and compressed medium based on multi-folded transformation are used to generate the open window and are embedded in the coating medium, making

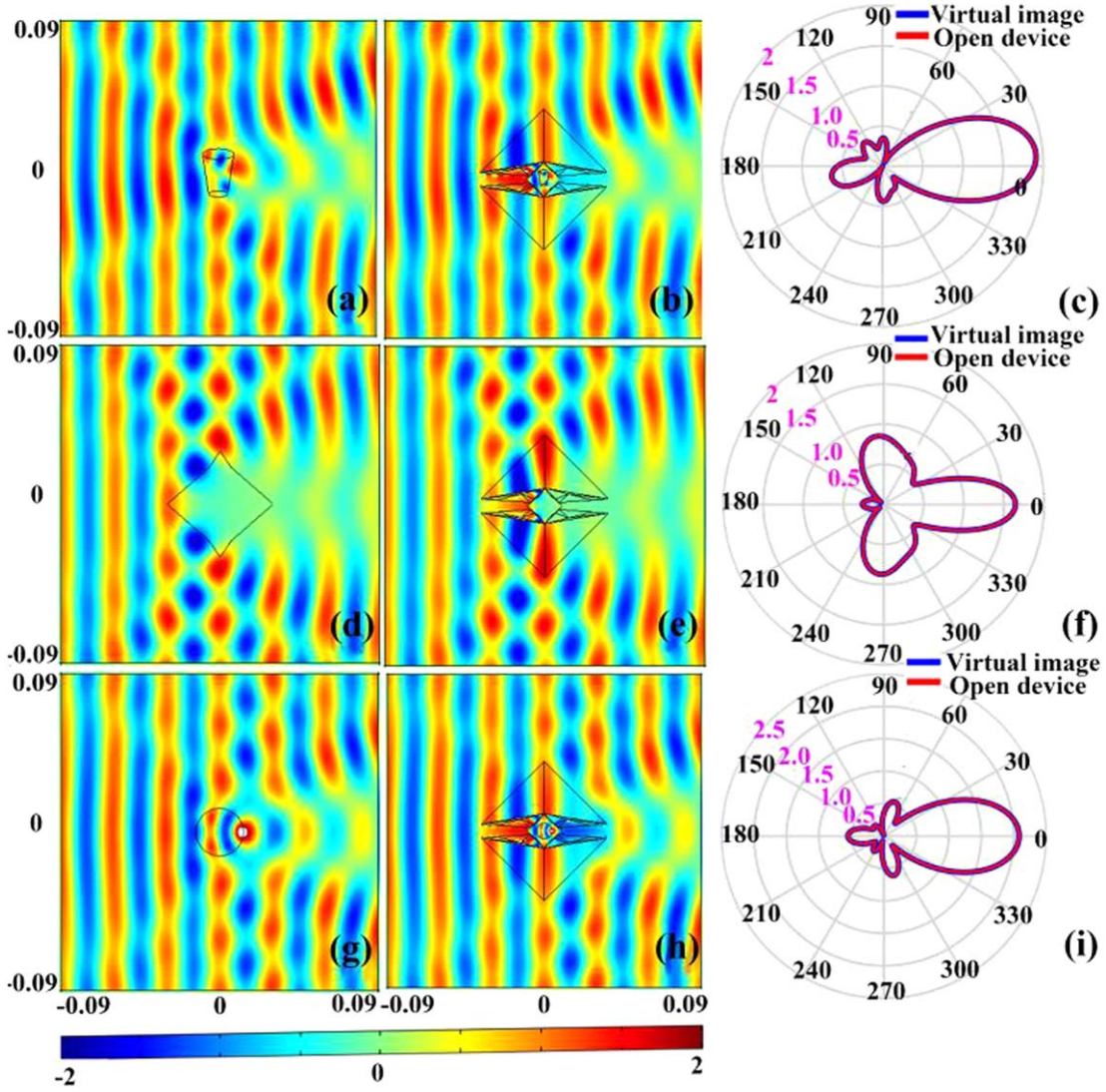

Figure 5. The Electric field (E_z) distributions of an object embedded in the proposed open amplifying device and its amplifying virtual image in the free space. A unit TE plane wave is irradiating on (a) a cup-shaped object with material parameters of $\varepsilon = 5$, $\mu = 1$, (d) a star-shaped object with material parameters of $\varepsilon = -1/9$, $\mu = 1$, (g) a circular-shaped object with material parameters of $\varepsilon = 3$, $\mu = 1$. The same TE Plane wave is irradiating on a small (b) cup- shaped object with material parameters of $\varepsilon = 45$, $\mu = 1$, (e) star-shaped object with material parameters of $\varepsilon = -1$, $\mu = 1$, (h) circular-shaped object with material parameters of $\varepsilon = 27$, $\mu = 1$ embedded in the proposed open amplifying device. (c) The far field differentials RCS of (a) and (b). (f) The far field differentials RCS of (d) and (e). (i)the far field differentials RCS of (g) and (h).

the open devices proposed here have a much compact, stable and robust structure than that of the previously remote devices. The open cloak has the capability to hide objects with arbitrary shapes, sizes and positions. The open concentrator enhances the EM energy in a core medium which is opened to the outer world. The open amplifying device magnifies the scattering field of an object that is embedded in the core material and renders the object to look like another object with a larger size and other parameters. The simulation results validate the effectiveness of the proposed devices. Although it still a challenge to realize such open devices at high EM band, we believed that the scheme presented here could be extended to other EM devices design and promoted the potential applications in remote control of microwave or optical engineering.

Acknowledgments

This work was funded by the National Natural Science Foundation of China (Grant Nos. 61461052, 11564044, 61863035), and was supported by the Key Program of Natural Science of Yunnan Province (Grant Nos. 2013FA006, 2015FA015).

ORCID iDs

Ming Huang https://orcid.org/0000-0002-9517-2125

References

[1] Pendry J B, Schurig D and Smith D R 2006 *Science* **312** 1780–2
[2] Leonhardt U 2006 *Science* **12** 1777–80
[3] Chen H Y, Chan C T and Sheng P 2010 *Nat. Mater.* **9** 387
[4] McCall M, Pendry J B, Galdi V, Lai Y, Horsley S A R, Li J and Ginis V 2018 *J. Opt.* **20** 063001
[5] Shin D, Kim J, Yoo D S and Kim K 2015 *Opt. Express* **23** 21892–8
[6] Jiang W X, Bao D and Cui T J 2016 *J. Opt.* **18** 044022
[7] Schurig D, Mock J J, Justice B J, Cummer S A, Pendry J B, Starr A F and Smith D R 2006 *Science* **314** 977–80
[8] Wu Q, Zhang K, Meng F Y and Li L W 2008 *J. Phys. D: Appl. Phys.* **42** 035408
[9] Li C, Meng X, Liu X, Li F, Fang G, Chen H and Chan C T 2010 *Phys. Rev. Lett.* **105** 233906
[10] Chen Z S, Mei Z L, Jiang W X and Cui T J 2018 *J. Phys. D: Appl. Phys.* **51** 155106
[11] Zheng B, Zhu R, Jing L, Yang Y, Shen L, Wang H and Chen H 2018 *Adv. Sci.* **5** 1800056
[12] Lai Y, Chen H Y, Zhang Z Q and Chan C T 2009 *Phys. Rev. Lett.* **102** 093901
[13] Chen H Y, Luo X D, Ma H R and Chan C T 2008 *Opt. Express* **16** 14603–8
[14] Yang C F, Huang M, Yang J J, Li T H, Mao F C and Li P 2019 *Opt. Commun* **435** 150–8
[15] Rahm M, Schurig D, Roberts D A, Cummer S A, Smith D R and Pendry J B 2006 *Photonic. Nanostruct.* **6** 87–95
[16] Pang X D and Zhu S Z 2013 *J. Electron. Inform. Tech.* **35** 468–73
[17] Li W, Guan J G and Wang W 2011 *J. Phys. D: Appl. Phys.* **44** 125401
[18] Madni H A, Hussain K, Jiang W X, Liu S, Aziz A, Iqbal S and Cui T J 2018 *Sci. Rep.* **8** 9641
[19] Lai Y, Ng J, Chen H Y, Han D, Xiao J, Zhang Z Q and Chan C T 2009 *Phys. Rev. Lett.* **102** 253902
[20] Shoorian H R and Abrishamian M S 2013 *J. Opt.* **15** 055107
[21] Madni H A, Zheng B, Akhtar M, Jaleel F, Liu S, Mahboob A and Cui T J 2019 *J. Opt.* **21** 035104
[22] Du Y, Zang X, Shi C, Ji X and Zhu Y 2015 *J. Opt.* **17** 025606
[23] Mei J S, Wu Q, Zhang K, He X J and Wang Y 2016 *Opt. Commun.* **368** 113–8
[24] Liu Y, Liang Z, Liu F, Diba O, Lamband A and Li J 2017 *Phys. Rev. Let.* **119** 034301
[25] Yang C F, Huang M, Yang J J, Mao F C and Li T H 2018 *Opt. Express* **26** 24280–93
[26] Yang C F, Huang M, Yang J J and Mao F C 2018 *Sci. Rep.* **8** 17339
[27] Yang T, Chen H Y, Luo X D and Ma H R 2008 *Opt. Express* **16** 18545–50
[28] Luo X D, Yang T, Gu Y W, Chen H Y and Ma H R 2009 *Appl. Phys. Lett.* **94** 223513
[29] Luo Y, Zhang J, Ran L, Chen H and Kong J A 2008 *IEEE Antenn. Wirel. Pr.* **7** 509–12
[30] Tang W X, Jiang W X and Cui T J 2014 *IEEE Antenn. Wirel. Pr.* **13** 1792–5
[31] Sedeh H B, Fakheri M H and Abdolali A 2019 *J. Opt.* **21** 045108
[32] Ebrahimpouri M and Quevedo-Teruel O 2017 *IEEE T. Antenn. Propag.* **65** 2256–64
[33] Barati H, Fakheri M H and Abdolali A 2018 *J. Opt.* **20** 085101
[34] Barati H, Basiri Z and Abdolali A 2018 *Chinese Phys. Lett.* **35** 104301
[35] Eskandari H, Majedi M S, Attari A R and Quevedo-Teruel O 2019 *New J. Phys.* **21** 063010
[36] Han T C, Qiu C W and Tang X H 2010 *Appl. Phys. Lett.* **97** 124104
[37] Han T C, Qiu C W and Tang X H 2010 *Opt. Lett.* **35** 2642–4
[38] Han T C, Qiu C W and Tang X H 2010 *J. Electromagn. Waves Appl.* **24** 1839–47
[39] Zheng B, Madni H A, Hao R, Zhang X, Liu X, Li E and Chen H S 2016 *Light-Sci. Appl.* **5** e16177
[40] Pendry J B, Holden A J, Stewart W J and Youngs I 1996 *Phys. Rev. Lett.* **76** 4773–6
[41] Pendry J B, Holden A J, Robbins D J and Stewart W J 1999 *IEEE T. Microw. Theory* **47** 2075–84
[42] Lai A, Itoh T and Caloz C 2004 *IEEE Microw. Mag.* **5** 34–50
[43] Caloz C and Itoh T 2005 *Electromagnetic Metamaterials: Transmission Line Theory and Microwave Applications* (New Jersey: John Wiley & Sons) (https://doi.org/10.1002/0471754323)
[44] Vakil A and Engheta N 2011 *Science* **332** 1291–4
[45] Chen T H, Zheng B, Yang Y H, Shen L, Wang Z, Gao F and Chen H 2019 *Light- Sci. Appl.* **8** 30